Mineralogical Magazine, August 1999, Vol. 63(4), pp. 559–566

Surface oxidation studies of chalcopyrite and pyrite by glancing-angle X-ray absorption spectroscopy (REFLEXAFS)

K. E. R. ENGLAND[1], J. M. CHARNOCK[1,2], R. A. D. PATTRICK[1] AND D. J. VAUGHAN[1]

[1] Department of Earth Sciences, University of Manchester, Manchester M13 9PL, UK
[2] CCLRC Daresbury Laboratory, Warrington WA4 4AD, UK

ABSTRACT

The oxidation of chalcopyrite and pyrite was examined using Fe-*K*- and Cu-*K*-edge REFLEXAFS spectroscopy. The Fe XANES of the pyrite proved to be a very sensitive indicator of oxidation, revealing the development of a goethite-like surface species; the EXAFS data showed an increasing O:S ratio with the degree of oxidation and gave Fe–O distances of *c.* 1.9 Å. On the oxidized chalcopyrite surfaces, the development of Fe-O and Cu-O species was observed, with both the XANES and EXAFS revealing the progressive development of these species with oxidation. Differences in the sensitivity of the XANES and EXAFS to the degree of oxidation can be related to the degree of long range order and changes in the intensity of the pre-edge feature of the Fe are a function of its oxidation state and coordination geometry in the surface species.

KEYWORDS: REFLEXAFS, pyrite, chalcopyrite, surface oxidation, XANES, EXAFS.

Introduction

THE oxidation of chalcopyrite and pyrite in aqueous solution is of importance in environmental geochemistry, in the hydrometallurgical processing of ores, and in flotation processing of ores and (for pyrite) coals. Numerous studies of pyrite oxidation under a wide range of conditions have been undertaken, and there has been a significant number of studies of the oxidation of chalcopyrite. In particular, the electrochemical oxidation and reduction of the chalcopyrite surface has been studied by Gardner and Woods (1979), Parker *et al.* (1981*a*,*b*); Warren *et al.* (1982); McMillan *et al.* (1982); Kelsall and Page (1984); Biegler and Horne (1985); Cattarin *et al.* (1990); and Yin *et al.* (1995). Amongst the many studies of electrochemical and aqueous oxidation of pyrite are Biegler and Swift (1979), McKibben and Barnes (1986), Moses *et al.* (1987), Mishra and Osseo-Asare (1992), Moses and Herman (1991), Tao *et al.* (1994), Williamson and Rimstidt (1994) and Kelsall *et al.* (1996). Earlier work was reviewed by Lowson (1982). These studies have identified several species on the surface of chalcopyrite including CuS_2^*, S, Fe_2O_3 and CuO (e.g. Yin *et al.*, 1995). The ions Fe^{2+}, Fe^{3+}, HSO_4^-, SO_4^{2-} and elemental S have been recognized on the surface of pyrite (e.g. Kelsall *et al.*, 1996).

Despite these and many other studies, detailed aspects of the mechanisms, rates, end- and intermediate-products of aqueous oxidation of chalcopyrite and pyrite remain poorly characterized and understood. This is partly due to the complex chemistries of the systems involved, but it is also because of the difficulties in determining directly the nature of the initial and intermediate products of oxidation reactions at the sulphide mineral-aqueous solution interface.

X-ray absorption spectroscopy employs synchrotron radiation as a source of high intensity X-rays (Koningsberger and Prins, 1988). The technique is element specific and has been widely used in mineralogical studies (Henderson *et al.*, 1995). The XAS spectrum can be divided into two regions, the X-ray absorption near edge structure (XANES) and the extended X-ray absorption fine structure (EXAFS). The XANES region is very sensitive to the coordination environment of the absorber atom and is often used as a 'fingerprinting' technique; the EXAFS region provides

information about bond lengths and coordination number. REFLEXAFS (Reflection Extended X-ray Absorption Fine Structure) is an extension of the standard EXAFS technique, in which the X-ray beam is incident upon the sample at a glancing angle, making it a surface sensitive technique (Greaves, 1991).

In the present study, we employ REFLEXAFS to study oxidized surfaces of chalcopyrite and pyrite. The objectives of the present work were to provide new data on the products of aqueous oxidation of chalcopyrite and pyrite under controlled conditions thereby evaluating the REFLEXAFS technique as a method of studying the surface oxidation of sulphide minerals.

Experimental details

Slices of polycrystalline chalcopyrite (from Palabora, South Africa) and single crystal ((100) face) pyrite (from Niccioletta, Tuscany) measuring ~40 × 30 mm^2 in area, and up to 5 mm thick, were mounted onto glass slides and polished to produce an optically flat surface. The samples were then oxidized electrochemically under controlled conditions, in 0.1 M $Na_2B_4O_7$ or 1 M $HClO_4$ solutions at various potentials and for various periods of time as indicated in Table 1. After preparation, the samples were stored under vacuum until required for analysis. The XAS data were acquired in air and therefore some further oxidation could have taken place during the experimental runs. However, the data obtained on the unoxidized sulphide samples suggested no detectable oxidation had taken place in addition to that produced by the electrochemical preparation.

The Fe-*K*-edge and Cu-*K*-edge REFLEXAFS measurements were obtained on Station 9.3 at the CCLRC Daresbury Laboratory Synchrotron Radiation Source, operating at 2 GeV with an average current of 150 mA. A Si(220) double crystal monochromator was used, detuned to reject 50% of the signal in order to minimize harmonic contamination. Full details of the REFLEXAFS experimental set-up can be found in Greaves (1991) and a schematic diagram of the experimental layout is shown in Fig. 1. For each sample a reflectivity curve was measured from which the critical angle was obtained. The REFLEXAFS data were collected with the angle of incidence, φ, (in millidegrees) set to ~½ the critical angle (in a smooth portion of the reflectivity curve), where the penetration depth would be 20–25 Å (Greaves, 1991), and also, in some cases, at angles greater than the critical angle (where the penetration depth is of the order

TABLE 1. *Details of conditions used to oxidize the samples used for REFLEXAFS measurements*

Sample	Oxidation conditions + calculated depth of oxidation
Pyrite — lightly oxidized	0.1 M $Na_2B_4O_7$ (pH 9.2) at 0.4 V *vs* SCE for 20 s Charge passed — 212 mC cm^{-2}
Pyrite — heavily oxidized	0.1 M $Na_2B_4O_7$ (pH 9.2) at 0.4 V *vs* SCE for 1.5 h Charge passed — 15.6 C cm^{-2}
Chalcopyrite — lightly oxidized	1 M $HClO_4$ at 0.6 V *vs* SCE for 2.5 h Charge passed — 0.27 C cm^{-2}
Chalcopyrite — moderately oxidized	0.1 M $Na_2B_4O_7$ (pH 9.2) at 0.4 V *vs* SCE for 2 h Charge passed — 0.77 C cm^{-2}
Chalcopyrite — heavily oxidized	0.1 M $Na_2B_4O_7$ (pH 9.2) at 1.5 V (between working electrode and Pt counter electrode) for 7 min Charge passed — 1.007 C cm^{-2}

SCE = Saturated Calomel Electrode

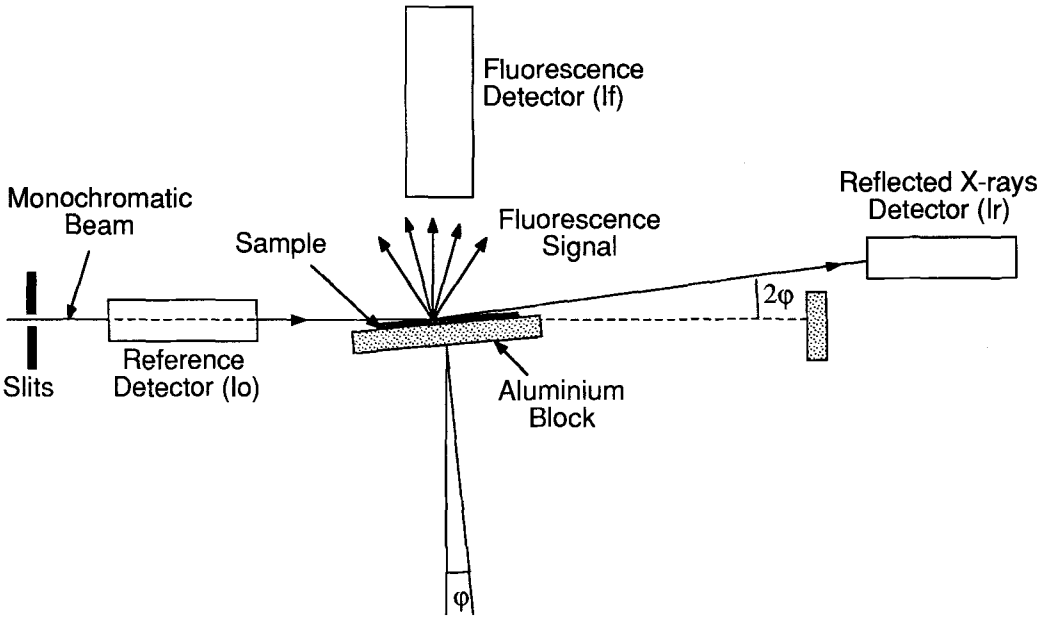

FIG. 1. Schematic drawing of the fluorescence REFLEXAFS experimental setup. *Io* = incident radiation, *If* = fluorescence signal, *Ir* = reflected radiation and φ = angle of incidence (after Greaves *et al.*, 1989).

of 100s of Å). At these higher angles, the signal due to atoms deeper within the sample contributes less to the total than that from those near the surface. This is due to attenuation of the incident beam through the sample, and to self-absorption by the sample of the fluorescence signal. For the concentrated samples analysed here, the latter effect will also distort the spectrum, reducing the intensity of the EXAFS oscillations. At angles less than the critical angle (i.e. X-ray penetration depth *c.* 25 Å), attenuation of the incident X-ray beam and fluorescence signal is negligible and therefore all atoms contribute equally to the spectrum. The fluorescence signal was collected using a Canberra 13-element solid state detector mounted above the sample, approximately ⊥ the plane of the surface.

Two to eight scans were collected and added together for each angle of incidence. The background subtracted data were processed using EXCURV92 (Binsted *et al.*, 1991). Phaseshifts were calculated *ab initio* using Hedin-Lundqvist potentials (Hedin and Lundqvist, 1969). The best theoretical fit to the data was obtained by adding shells of backscatterers around the central absorber atom, and iterating the absorber-scatterer distances, *R*, and the Debye-Waller factors, $2\sigma^2$ (Gurman *et al.*, 1984). The Debye-Waller factors are a function of the relative motion between the central atom and the scatterer, and also of small variations in distance of the atoms within a shell from the central atom.

Results

The REFLEXAFS data for pyrite are presented in Table 2 and Figs 2 and 3. Unoxidized, slightly oxidized and heavily oxidized pyrites were examined at different angles of incidence. The XANES show clear spectral differences between the samples. In the pre-edge region the feature at 7106.5 eV is largest in the least oxidized sample and decreases with increasing degree of oxidation. The changes in the remaining features of the XANES spectra at ½ the critical angle (Fig. 2), also exhibit a progression from unoxidized pyrite to the most highly oxidized sample, and reflect the development on the surface of a phase which has spectral characteristics similar to those of goethite. The spectra collected at angles >½ the critical angle are closer to that of unaltered pyrite (Fig. 2).

The best fits from the analyses of the Fe-*K*-edge EXAFS data from the pyrite samples are given in

TABLE 2. Best fit parameters for the pyrite REFLEXAFS spectra at the Fe-*K*-edge

Sample and angle of incidence	Scatterer	*N*	*R*/Å	$2\sigma^2$/Å^{2†}
Unaltered surface, 172 mdeg	S	6	2.24	0.005
Unaltered surface, 680 mdeg	S	6	2.24	0.025
Lightly oxidized, 140 mdeg	S	4	2.20	0.005
	O	2	1.85	0.002
Lightly oxidized, 350 mdeg	S	6	2.22	0.011
Heavily oxidized, 140 mdeg	S	2	2.25	0.014
	O	4	1.90	0.002
Heavily oxidized, 280 mdeg	S	2	2.14	0.062
	O	4	1.98	0.028
Heavily oxidized, 560 mdeg	S	4	2.18	0.074
	O	2	2.01	0.008

N = coordination number, *R* = first shell distance (±0.02 Å) and $2\sigma^2$ = Debye-Waller factor (±20%†).
†For angles >½ the critical angle, the Debye-Waller factor is exaggerated.

Table 2. Each spectrum was initially simulated by using a shell of six S atoms at *c.* 2.3 Å, and varying the distance and Debye-Waller factor to get the best fit. Oxygen atoms at *c.* 2.0 Å were then added, reducing the S coordination number to maintain a total coordination of six; the distances and Debye-Waller factors were again iterated. The Joyner statistical test (Joyner *et al.*, 1987) was used to determine whether the improvement in fit justified the additional parameters. In each case the model which gave the best fit (i.e. with the lowest residual, *R*) is shown in Table 2. The unoxidized pyrite Fe-*K*-edge EXAFS spectrum collected at ½ the critical angle is identical to that for bulk FeS_2. The best fit for the lightly oxidized pyrite at ½ the critical angle is obtained with 4 sulphurs and 2 oxygens, and for the heavily oxidized pyrite, the best fit suggests an average coordination of 2 sulphurs and 4 oxygens surrounding the Fe. For angles greater than the critical angle the spectra are noticeably distorted due to self-absorption effects (Koningsberger and Prins, 1988). Although this distortion reduces the amplitude of the EXAFS oscillations which results in unrealistically high Debye-Waller factors, it has no effect on the frequency of the oscillations, and therefore the bond lengths can be utilized. At these higher angles, the ratio of S:O in the coordination sphere around the Fe increases. In the case of the heavily oxidized sample analysed at the critical angle, the S:O ratio is the same as for the sample at ½ the critical angle, reflecting the deeper oxidation. All

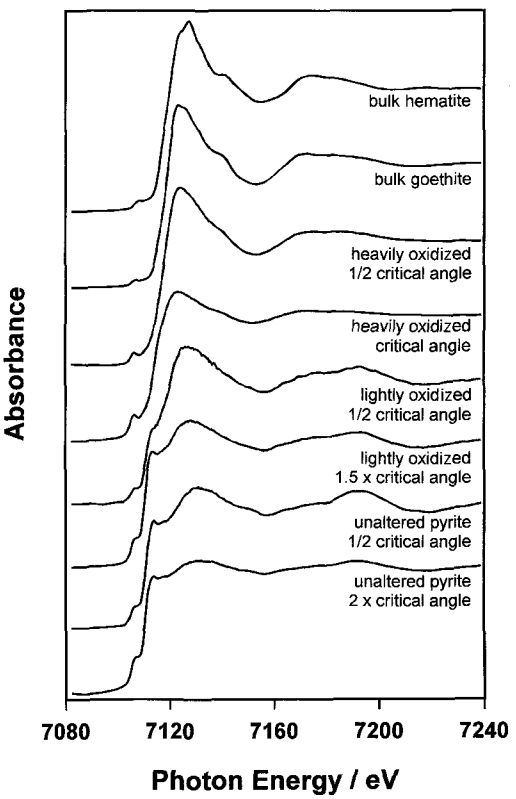

FIG. 2. Fe-*K*-edge XANES of pyrite surfaces collected at angles as indicated. Spectra of bulk goethite (FeO.OH) and hematite are shown for comparison.

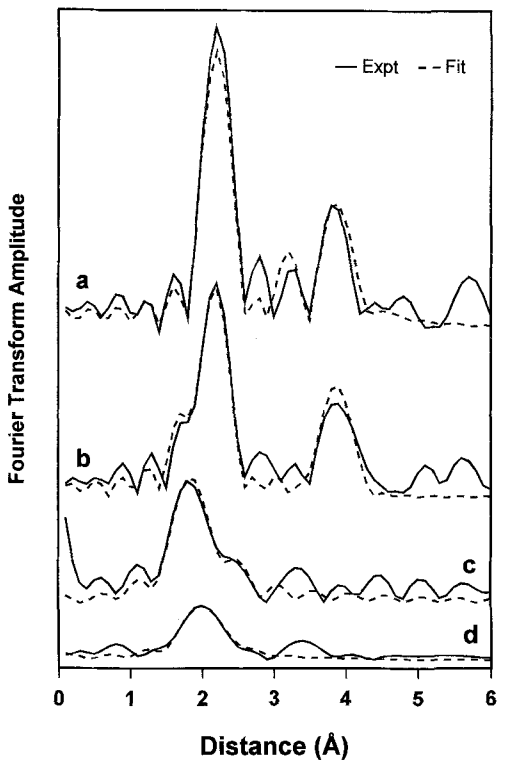

FIG. 3. Fourier transforms of the k^3-weighted Fe-*K*-edge REFLEXAFS spectra: (a) unoxidized surface; (b) lightly oxidized surface; (c) heavily oxidized surface, all at ½ the critical angle; and (d) heavily oxidized surface at the critical angle. The changing ratio of the peak due to O atoms in the inner coordination sphere at *c.* 1.9 Å and S atoms at 2.2 Å can be seen seen clearly.

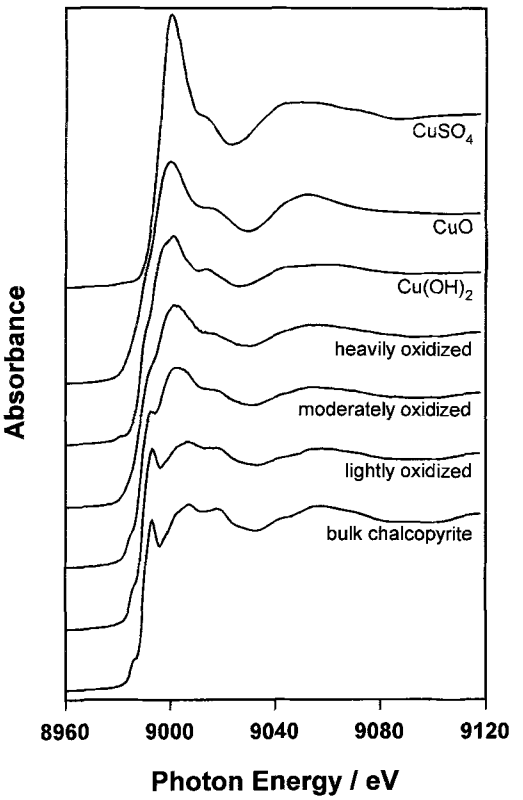

FIG. 4. Cu-*K*-edge XANES of oxidized chalcopyrite surfaces collected at ½ the critical angle. Spectra of bulk chalcopyrite, $Cu(OH)_2$, CuO, and $CuSO_4$ are shown for comparison.

these changes in the S:O ratio can be seen clearly as changes in the peak heights in the Fourier transforms of the Fe-*K*-edge EXAFS spectra (Fig. 3), with O atoms at ~1.9 Å and S atoms at ~2.2 Å.

The XANES of the Cu- and Fe-*K*-edge spectra derived from the chalcopyrite slabs measured at ½ the critical angle are presented in Figs 4 and 5 and analysis of the EXAFS data in Tables 3 and 4; data from a powdered bulk sample are shown for comparison. From the Cu XANES data it is clear that the lightly oxidized sample resembles the bulk sample, but the heavily oxidized sample is quite different, with the moderately oxidized sample intermediate. These Cu XANES spectra show clear trends from the unoxidized to the highly oxidized samples illustrated by the progressive loss of the pre-edge feature and a loss in resolution of the feature at 8993 eV. At the Fe-*K*-edge there are changes in edge profile, although the pre-edge feature is only slightly reduced and the moderately oxidized sample is very similar to the heavily oxidized sample.

The Cu- and Fe-*K*-edge EXAFS data were analysed using the same method as for pyrite, except that the total coordination number was maintained at four. At ½ the critical angle, even for the most heavily oxidized sample, no more than one O atom was required to obtain the best fit for both metal edges. For the lightly oxidized sample there was a slight improvement in fit at both edges on addition of the O shell, but in neither case was this statistically significant. For the moderately oxidized sample the improvement was significant for the Fe spectrum, but not the

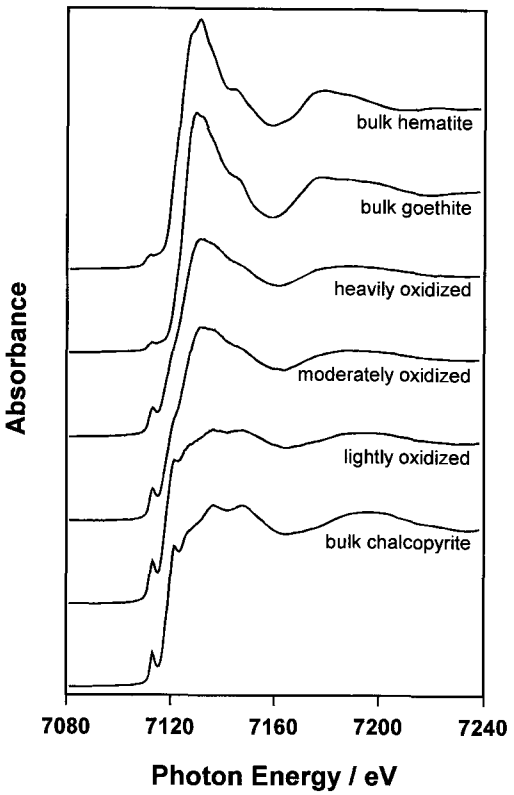

FIG. 5. Fe-*K*-edge XANES of oxidized chalcopyrite surfaces collected at ½ the critical angle. Spectra of bulk chalcopyrite, goethite and hematite are shown for comparison.

Cu, and for the heavily oxidized sample the improvement was significant at both edges.

The Cu- and Fe-*K*-edge EXAFS spectra were also collected from the same chalcopyrite samples at twice the critical angle. These revealed that even for the most oxidized sample, no O was apparent in the Cu coordination sphere and in the case of the Fe-*K*-edge data O was present in only the most heavily oxidized sample.

Discussion

The oxidation of the pyrite and chalcopyrite is clearly evident from the improved fit on the addition of O in the EXAFS, with the more highly oxidized samples requiring more O atoms in the coordination sphere. Using the same reasoning, the decrease in the degree of oxidation with depth is also apparent from the data obtained at higher angles of incidence. The EXAFS also show that the surface layers of the most highly oxidized chalcopyrite contain some Cu-O and Fe-O species whereas in the less oxidized samples, and at depth, only Cu-S and Fe-S species are present. The Cu–O bond lengths derived from the oxidized surface are typical of those found in the inner coordination sphere of Cu(II) oxides, such as CuO and $Cu(OH)_2$ while the Fe–O distances are typical of Fe(III) oxides, such as hematite and goethite.

The XANES derived from the samples proved to be a sensitive indicator of the changes in the proportions of the sulphide and oxide species present. For pyrite the changes in the Fe-*K*-edge XANES reflect changes in the S:O ratios derived from the EXAFS. In the pre-edge region (Fig. 2), the feature at 7106.5 eV is assigned to a transition from the Fe 1*s* states to states which are mainly Fe $3d_{eg}$ in character (with some Fe 4*p* and S 3*p* or O 2*p* contribution) (Mosselmans *et al.*, 1995). As Fe is octahedrally coordinated in both pyrite and common Fe oxides, the change in intensity of the feature is due to a combination of a change in the oxidation state of the Fe and a change from low spin Fe (pyrite) to high spin Fe.

TABLE 3. Best fit parameters for the chalcopyrite REFLEXAFS spectra at the Cu-*K*-edge

Sample and angle of incidence	Scatterer	*N*	*R*/Å	$2\sigma^2$/Å^2
Bulk chalcopyrite	S	4	2.28	0.013
Lightly oxidized, 120 mdeg	S	4	2.29	0.019
Moderately oxidized, 115 mdeg	S	4	2.20	0.028
Heavily oxidized, 118 mdeg	S	3	2.21	0.023
	O	1	1.85	0.005

N = coordination number, *R* = first shell distance (±0.02 Å) and $2\sigma^2$ = Debye-Waller factor (±20%).

TABLE 4. Best fit parameters for the chalcopyrite REFLEXAFS spectra at the Fe-*K*-edge

Sample and angle of incidence	Scatterer	*N*	*R*/Å	$2\sigma^2$/Å^2
Bulk chalcopyrite	S	4	2.26	0.007
Lightly oxidized, 150 mdeg	S	4	2.26	0.012
Moderately oxidized, 125 mdeg	S	3	2.22	0.016
	O	1	1.93	0.018
Heavily oxidized, 160 mdeg	S	3	2.23	0.017
	O	1	1.93	0.017

N = coordination number, R = first shell distance ($\pm$0.02 Å) and $2\sigma^2$ = Debye-Waller factor ($\pm$20%).

However, in the case of the most heavily oxidized chalcopyrite, for which the EXAFS yielded a relatively high S:O ratio of 3:1, the XANES have largely lost the chalcopyrite characteristics and resemble more closely the oxide species (Fig. 5). The pre-edge feature in these chalcopyrite Fe-K-edge spectra also loses some intensity with increased oxidation but, in contrast to peaks just above the absorption edge, the decrease corresponds to the changes in S:O ratio seen in the EXAFS. As the Fe in chalcopyrite is Fe(III), there is no change in oxidation state and in this case the change in the pre-edge feature can be related to the increase from tetrahedral (chalcopyrite) to octahedral coordination. The contrast in the changes in behaviour between the XANES and the pre-edge feature can, in part, simply reflect the higher intensity of the XANES peaks of the oxide species. However, it may also reflect the loss of the long range order in chalcopyrite as it suffers oxidative breakdown. This would have less effect on the pre-edge feature which is due to the 1*s* to 3*d* transition, than on the XANES peaks which contain contributions from multiple scattering. Also, as we only see the inner coordination sphere in the EXAFS of the chalcopyrite, this will be insensitive to the degree of long range order. This may explain why the effect on the XANES of a small change in the S:O ratio from 4:0 to 3:1 is much greater than that on the EXAFS.

Using the XAS data to make a definitive identification of the species produced by oxidation proved difficult. The metal–oxygen bond lengths are typical of all of the oxide species that might form and therefore cannot be used to discriminate between species. The Fe-*K*-edge XANES of the heavily oxidized sulphide surfaces suggest that the same Fe-O species is present on both the chalcopyrite and pyrite. When compared with the XANES of other iron oxides, they can be seen to most closely resemble goethite, although both hematite and goethite have similar XANES spectra (Figs 2 and 4). The Cu-*K*-edge XANES of the most oxidized chalcopyrite show similarities to the XANES of Cu-O compounds, especially $Cu(OH)_2$ (Fig. 4); if CuS or CuS_2 was formed at the surface it could not be differentiated from the chalcopyrite contribution to the XAS data.

In summary, the XANES proved to be a sensitive indicator of oxidation, and accurate bond distances have been obtained for the reaction products from the EXAFS analyses. This type of information can be used in combination with information from other techniques to identify surface species. In this study the identification of the species proved difficult, inhibited by the one of the drawbacks of XAS analysis, namely the inability to differentiate between species in mixed systems. The Fe-S-Cu-O-(H) system is particularly complex and therefore several chemically similar species can be present, reducing the possibility of a unique interpretation. However, in simpler systems or in systems where reactions involve surface species that are distinct from the substrate (i.e. sorption, activation or replacement), definitive results can be obtained using REFLEXAFS and, as this study demonstrates, both the XANES and the EXAFS will reflect the changing surface environment.

Acknowledgements

We are grateful to Q. Yin for preparation of the samples and to J.F.W. Mosselmans for helpful interruptions. The Director of the CCLRC Daresbury Laboratory and EPSRC are thanked for the provision of beamtime on the SRS.

References

Biegler, T. and Horne, M.D. (1985) The electrochemistry of surface oxidation of chalcopyrite. *J. Electrochem. Soc.*, **32**, 1363–9.

Biegler, T. and Swift, D.A. (1979) Anodic behaviour of pyrite in acid solutions. *Electrochim. Acta*, **24**, 415–20.

Binsted, N., Campbell, J.W., Gurman, S.J. and Stephenson, P.C. (1991) Daresbury Laboratory EXCURV92 program.

Cattarin, S., Flechter, S., Pettenkofer, C. and Tributsch, H. (1990) Interfacial reactivity and oscillating behavior of chalcopyrite cathodes during H_2O_2 reduction II. Characterisation of electrode corrosion. *J. Electrochem. Soc.*, **137**, 3484–93.

Gardner, J.R. and Woods, R. (1979) An electrochemical investigation of the natural flotability of chalcopyrite. *Int. J. Miner. Proc.*, **6**, 1–16.

Greaves, G.N. (1991) Glancing angle X-ray absorption spectroscopy. *Advances X-ray Anal.*, **34**, 13–22.

Greaves, G.N., Barrett, N.T., Antonini, G.M., Thornley, F.R., Willis, B.T.M. and Steel, A. (1989) Glancing-angle X-ray absorption spectroscopy of corroded borosilicate glass surfaces containing uranium. *J. Amer. Chem. Soc.*, **111**, 4313–24.

Gurman, S.J., Binsted, N. and Ross, N. (1984) A rapid, exact, curved wave theory for EXAFS calculations. *J. Phys. C*, **17**, 143–51.

Hedin, L. and Lundqvist, S. (1969) Effects of electron-electron and electron-phonon interactions on the one-electron states of solids. *Solid State Phys.*, **23**, 1–181.

Henderson, C.M.B., Cressey, G. and Redfern, S.A.T. (1995) Geological applications of synchrotron radiation. *Radiat. Phys. Chem.*, **45**, 459–81.

Joyner, R.W., Martin, K.J. and Meehan, P. (1987) Some applications of statistical tests in analysis of EXAFS, SEXAFS and XANES. *J. Phys. C*, **20**, 4005–12.

Kelsall, G.H. and Page, P.W. (1984) Aspects of chalcopyrite ($CuFeS_2$) electrochemistry. In *International Symposium on Electrochemistry in Mining and Metallurgy Process* (P.E. Richardson *et al.*, eds), pp. 303–16. Electrochemical Society, New Jersey, USA.

Kelsall, G.H, Yin, Q., Vaughan, D.J. and England, K.E.R. (1996) Electrochemical oxidation of pyrite (FeS_2) in acidic aqueous electrolytes I. In *International Symposium on Electrochemistry in Mineral and Metal Processing* (R. Woods, P.E. Richardson and F.M. Doyle, eds), **96-6**, pp 131–42. Electrochemical Society, New Jersey, USA.

Koningsberger, D. and Prins, R. (eds) (1988) *X-ray Absorption: Principles, Applications, Techniques of EXAFS, SEXAFS and XANES.* Wiley, New York.

Lowson, R.T. (1982) Aqueous oxidation of pyrite by molecular oxygen. *Chem. Rev.*, **82**, 461–97.

McKibben, M.A. and Barnes, H.L. (1986) Oxidation of pyrite in low temperature acidic solutions: rate laws and surface textures. *Geochim. Cosmochim. Acta*, **50**, 1509–20.

McMillan, R.S., Mackinnon, D.J. and Dutriizac, J.E. (1982) Anodic dissolution of n-type and p-type chalcopyrite. *J. Appl. Electrochem.*, **12**, 743–57.

Mishra, K.K. and Osseo-Asare, K. (1992) Fermi-level spinning at pyrite (FeS_2)/electrolyte junctions. *J. Electrochem. Soc.*, **139**, 749–52.

Moses, C.O. and Herman, J.S. (1991) Pyrite oxidation at circumneutral pH. *Geochim. Cosmochim. Acta*, **55**, 471–82.

Moses, C.O., Nordstrom, D.K., Herman, J.S. and Mills, A.L. (1987) Aqueous pyrite oxidation by dissolved oxygen and by ferric iron. *Geochim. Cosmochim. Acta*, **51**, 1561–71.

Mosselmans, J.F.W., Pattrick, R.A.D., van der Laan, G., Charnock, J.M., Vaughan, D.J., Henderson, C.M.B. and Garner, C.D. (1995) X-ray absorption near-edge spectra of transition metal disulfides FeS_2 (pyrite and marcasite), CoS_2, NiS_2, and CuS_2 and their isomorphs FeAsS and CoAsS. *Phys. Chem. Mineral.*, **22**, 311–7.

Parker, A.J., Paul, P.L., and Power, G.P. (1981a) Electrochemical aspects of leaching copper from chalcopyrite in ferric and cupric salt solutions. *Australian J. Chem.*, **34**, 13–34.

Parker, A.J., Paul, P.L. and Power, G.P. (1981b) Electrochemistry of the oxidative leaching of copper from chalcopyrite. *J. Electroanal. Chem.*, **118**, 305–16.

Tao, D.P., Li, Y.Q., Richardson, P.E. and Yoon, R.H. (1994) *The incipient oxidation of pyrite. Colloids and Surfaces A. Physicochemical and Engineering Aspects*, pp. 229–39. Elsevier Science Publications, The Netherlands.

Warren, G.W., Wadsworth, M.E., and El-Raghy, S.M. (1982) Passive and transpassive anodic behaviour of chalcopyrite in acid solutions. *Met. Trans.*, **B13**, 571–9.

Williamson, M.A. and Rimstidt, J.D. (1994) The kinetics and electrochemical rate-determining step of aqueous pyrite oxidation. *Geochim. Cosmochim. Acta*, **58**, 5443–54.

Yin, Q., Kelsall, G.H., Vaughan, D.J. and England, K.E.R. (1995) Atmospheric and electrochemical oxidation of the surface of chalcopyrite ($CuFeS_2$). *Geochim. Cosmochim. Acta*, **59**, 1091–100.

[*Manuscript received 2 July 1998: revised 13 November 1998*]